ARTICLE

Oxidation Decomposition Mechanism of Fluoroethylene Carbonate-Based Electrolytes for High-Voltage Lithium Ion Batteries: A DFT Calculation and Experimental Study

Lan Xia,[a], [b], [1] Bencan Tang,[b], [1] Linbin Yao,[b] Kai Wang,[b] Anastasia Cheris,[b] Yueyang Pan,[b] Saixi Lee,[a] Yonggao Xia*[a], George Z. Chen,*[b] Zhaoping Liu[a]

Abstract: The oxidative decomposition mechanism of fluoroethylene carbonate (FEC) used in high-voltage batteries is investigated by using density functional theory (DFT). Radical cation FEC^{+} is formed from FEC by transferring one electron to electrode and the most likely decomposition products are CO_2 and 2-fluoroacetaldehyde radical cation. Other possible products are CO, formaldehyde and formyl fluoride radical cations. These radical cations are surrounded by much FEC solvent and their radical center may attack the carbonyl carbon of FEC to form aldehyde and oligomers of alkyl carbonates, which is similar with the oxidative decomposition of EC. Then, our experimental result reveals that FEC-based electrolyte has rather high anodic stability. It can form a robust SEI film on the positive electrode surface, which can inhibit unwanted electrolyte solvent and $LiPF_6$ salts decomposition, alleviate Mn/Ni dissolution and therefore, improve the coulombic efficiency and the cycling stability of high voltage $LiNi_{0.5}Mn_{1.5}O_4$ positive electrodes. This work displays that FEC-based electrolyte systems have considerable potential replacement of the EC-based electrolyte for the applications in 5 V Li-ion batteries.

Introduction

The demand for high-voltage positive electrode materials has become a high priority for the integration for high-energy density rechargeable lithium-ion batteries (LIBs) in transportation and grid load levelling. Recently, with the advantages of high operating voltage of ~4.7 V vs. Li^+/Li, high capacity of ~146.7 mAh g^{-1} and low cost, spinel $LiNi_{0.5}Mn_{1.5}O_4$ materials have been investigated extensively. However, a major difficulty in using these positive electrode materials is the capacity fade resulting from the oxidative instability of the conventional EC-based electrolyte at high operating potentials. [1-3]

[a] *Dr. L. Xia, S. Lee, Prof. Y.-G. Xia, Prof. Z.-P Liu*
Ningbo Institute of Materials Technology & Engineering (NIMTE)
Chinese Academy of Sciences (CAS)
Ningbo, Zhejiang, 315201, P. R. China
E-mail: xiayg@nimte.ac.cn

[b] *Dr. B. Tang, L. Yao, K. Wang, A. Cheris, Prof. G. Chen*
Department of Chemical and Environmental Engineering, and
Centre for Sustainable Energy Technologies, Faculty of Science and Engineering
University of Nottingham Ningbo China
Ningbo, Zhejiang, 315100, P. R. China
E-mail: George.Chen@nottingham.edu.cn

[1] *Lan Xia and Bencan Tang contributed equally to this work and should be considered as co-first authors.*

One of the most effective strategies to inhibit this issue is the development of novel stable solvents for high-voltage electrolyte solutions. Due to the high electronegativity and low polarizability of the fluorine atom, fluorinated solvents possess increased oxidative stability. Expect for its higher oxidation stability, the fluorinated solvents show higher flash point and lower melting point compared to the corresponding non-fluorinated solvents, and these properties can improve the safety and low-temperature performance, respectively. [4-6] Therefore, the FEC-based electrolyte (EC was totally replaced by FEC) has been used in high-voltage positive electrode materials. [3, 7-10] In 2010, Ishikawa et al [8] for the first time showed that the $Li/LiCoO_2$ cell containing the FEC-based electrolyte exhibited a higher and more stable discharge capacity even with a high upper cut-off of 4.5 V compared to the cell containing the EC-based electrolyte. In recent years, Zhang's group [9] reported that the FEC-based electrolyte improved the electrochemical performance of $LiNi_{0.5}Mn_{1.5}O_4$ at elevated temperature. The high oxidative stability of the fluorinated carbonate solvents-based electrolytes was supported by later electrochemical evaluation results using $LiNi_{0.5}Mn_{1.5}O_4/Li$ and $LiNi_{0.5}Mn_{1.5}O_4/Li_4Ti_5O_{12}$ cells. [3] Expert for using in high-voltage $LiNi_{0.5}Mn_{1.5}O_4$ materials, Markevich et al [10] reported a drastic improvement in the cycling stability of $LiCoPO_4$ cathodes in the FEC-based electrolytes. Although these FEC-based electrolyte systems provide excellent cycling stability on the high-voltage $LiNi_{0.5}Mn_{1.5}O_4$ materials, the chemical and physical properties of the interface film at the high-voltage positive electrode using fluorinated carbonate-based electrolyte has not yet been understood to the best of our knowledge. Furthermore, as far as we all know, the interfacial problems on the surface of positive electrodes is very important because they contribute to performance degradation of the battery upon cycling. [11-15] Thus, it is meaningful to clarify the oxidation decomposition mechanism of FEC-based electrolytes under high-voltage conditions.

Generally, the oxidative decomposition of solvents take place on the electrode surface, understanding the detailed mechanism on the oxidative decomposition of solvents is essential on order to choose appropriate electrolyte components compatible with electrode materials. Many density functional theory (DFT) calculations have been focused on understanding oxidative stability of solvents, [16-18] redox shuttle additives, [19-22] and anions [23, 24]. However, few works indicate that DFT studies can also be used to give the oxidative decomposition pathways of solvents. [12, 25, 26] For example, DFT studies of propylene carbonate (PC) [27] indicated that the calculated oxidative decomposition mechanism using a B3LYP/6-311++G (d) DFT level was found in

close agreement with the experimental findings reported in the literature, [28] and the calculation results clarified the role of intermediate propylene oxide in PC decomposition. Then, Leggesse [29] had shown that the B3LYP/6-311++G (d, p) level accurately reported that the oxidative decomposition products of PC were independent of the lithium salt type, while its rate constants were highly affected by the type of the lithium salt. This result indicated that DFT calculations at B3LYP/6-311++G (d, p) could be effectively used for studying the decomposition mechanism of solvents. In another example, the detailed oxidative decomposition mechanism of EC was investigated using DFT method at the level of B3LYP/6-311++G (d, p) by Xing et al. The result showed that there were five possible pathways for the decomposition of $EC^{\bullet+}$, result in forming CO_2, CO, and various radical cations, and finally lead to generate aldehyde and oligomers of alkyl carbonates including 2-methyl-1,3-dioxolane, 1,3,6-trioxocan-2-one, 1,4,6,9-tetraoxaspiro[4.4] nonane, and 1,4,6,8,11-pentaoxaspiro[4.6]undecan-7-one. [12] For these reason, in this paper, we firstly present the detailed oxidative decomposition mechanism of FEC with theoretical calculation using DFT at the level of B3LYP/6-311++G (d, p). Then, in experiment section, we focus on the effect of FEC in improving the cyclability and surface chemistry of $LiNi_{0.5}Mn_{1.5}O_4$ high-voltage materials through the combined use of scanning electron microscopy (SEM), electrochemical impedance spectroscopy (EIS), and X-ray photoelectron spectroscopy (XPS).

Results and Discussion

In order to understand the oxidative decomposition mechanism of FEC, our calculation was started from radical cation **$FEC^{\bullet+}$**, which was formed from FEC by transferring one electron to electrode. The optimized geometry of **EC, FEC, EMC, PF_6^-** and initial oxidative products (**$FEC^{\bullet+}$**, **Int_{C1}**, **Int_{E1}**, **Int_{E2}**, **Int_{E3}**) of **$FEC^{\bullet+}$** are shown in Figure 1. Li group carried out a thorough theoretical investigation of the oxidative decomposition mechanism of ethylene carbonate (EC) for lithium ion battery. [12] FEC is different from EC in that it is not a symmetric structure. Therefore, **$FEC^{\bullet+}$** can decompose in five possible pathways, i.e. pathway A-E in Figure 2, through five transition states (**TS_{A1-E1}**), leading to five initial products (**Int_{A1-E1}**), as shown in Figure 2. Our theoretical result is similar to Li group's report for **$EC^{\bullet+}$**, in that the decomposition barrier in pathway D (**TS_{D1}** 13.5 kcal mol^{-1}) and E (**TS_{E1}** 9.6 kcal mol^{-1}) is lower than that in A (**TS_{A1}** 31.6 kcal mol^{-1}) and B (**TS_{B1}** 39.1 kcal mol^{-1}) for **$FEC^{\bullet+}$**, which were 9.6 kcal mol^{-1} and 38.7 kcal mol^{-1} for breaking (O=)C-O and (F)C-O bonds respectively in **$EC^{\bullet+}$** [12]. It is worth to mention that **TS_{B1}** can lead to the final product CO_2 and acetyl fluoride directly without any other transition states. The difference in the decomposition of **$FEC^{\bullet+}$** and **$EC^{\bullet+}$** is that, for **$FEC^{\bullet+}$**, the cyclic C-C bond can also easily break (**TS_{C1}**) with an activation energy only 11.4 kcal mol^{-1}, making this the second favorable path in the decomposition of **$FEC^{\bullet+}$**. The resultant intermediate Int_{C1} can decompose in two different ways through **TS_{C2}** (ΔG 12.8 kcal mol^{-1}) and **TS_{C4}** (ΔG 11.7 kcal mol^{-1}) respectively, leading to **Int_{C2}** and **Int_{C4}** separately. **Int_{C2}** can further decompose through **TS_{C3}** (ΔG 9.3 kcal mol^{-1}) to **Int_{C3}**, which is a complex formed by CO, formyl fluoride and formaldehyde. **Int_{C4}** was expected to decompose to form **Int_{C5}** directly through a transition state, such as **TS_{C5}**. However, we could not find such a transition state to connect **Int_{C4}** and **Int_{C5}**, but only a transition state leading to **Int_{C2}**, which can be optimized to different minimums with deferent energies (see Figure 3) and degree of linearity of O=C-O bond. The most favorable decomposition is through pathway E, with a barrier of only 9.6 kcal mol^{-1} and, after breaking two more bonds through **TS_{E2}** (ΔG 4.9 kcal mol^{-1}) and **TS_{E3}** (ΔG 3.8 kcal mol^{-1}), leads to very stable product CO_2 and 2-fluoroacetaldehyde.

Based on the above calculation, pathway E would be the most probable reaction for the decomposition of **$FEC^{\bullet+}$**, followed by pathway C, path D, path A, and path B. the most likely decomposition products are CO_2 and 2-fluoroacetaldehyde (through pathway E). Other possible products are CO, formaldehyde and formyl fluoride (pathway C); acetyl fluoride and 2-fluorooxirane are less likely formed due to much higher decomposition barriers in pathway A and B. These initial products should be include the **Int_{E1}**, **Int_{E2}** and **Int_{E3}** radical cations. Considering these radical cations are surrounded by much FEC, their radical center may attack the carbonyl carbon of FEC to form aldehyde and oligomers of alkyl carbonates, which is agreement with the reported results [12]. The calculation also indicates that FEC is thermodynamically more stable than its non-fluorinated counterparts EC under certain high voltage conditions, as shown in Table S1. We carried out the experimental methods to investigate the properties of the FEC-based electrolyte in high-voltages batteries in the following section.

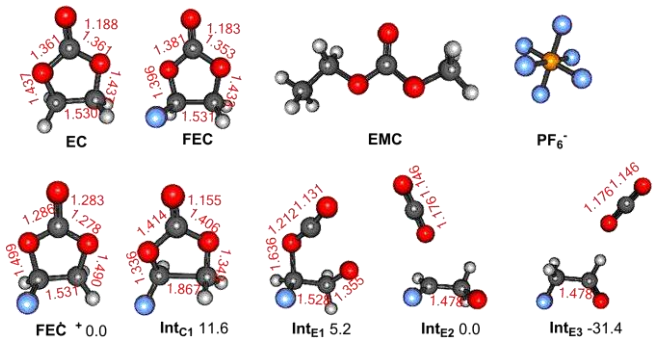

Figure 1. The optimized geometry of **EC, FEC, EMC, PF_6^-** and initial oxidative products (**$FEC^{\bullet+}$, Int_{C1}, Int_{E1}, Int_{E2}, Int_{E3}**) of $FEC^{\bullet+}$ at B3LYP/6-311++G (d, p) level. Computed free energy profile (Grel, 298K) kcal mol^{-1}. Bond lengths are in angstrom.

.

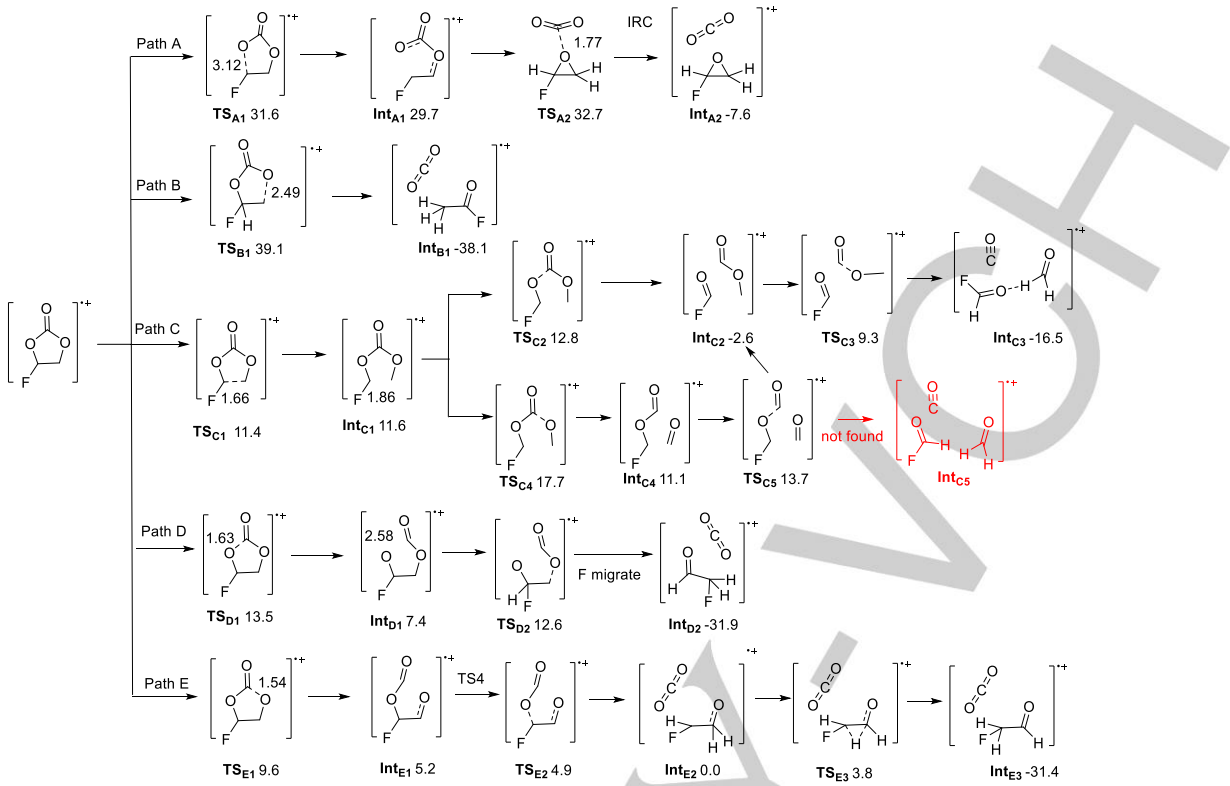

Figure 2. Possible pathways for decomposition of **FEC$^{\bullet+}$**. Computed free energy profile (Grel, 298K) kcal mol^{-1}. Energy was estimated using B3LYP/6-311++G (d, p) level. Bond lengths are in angstrom.

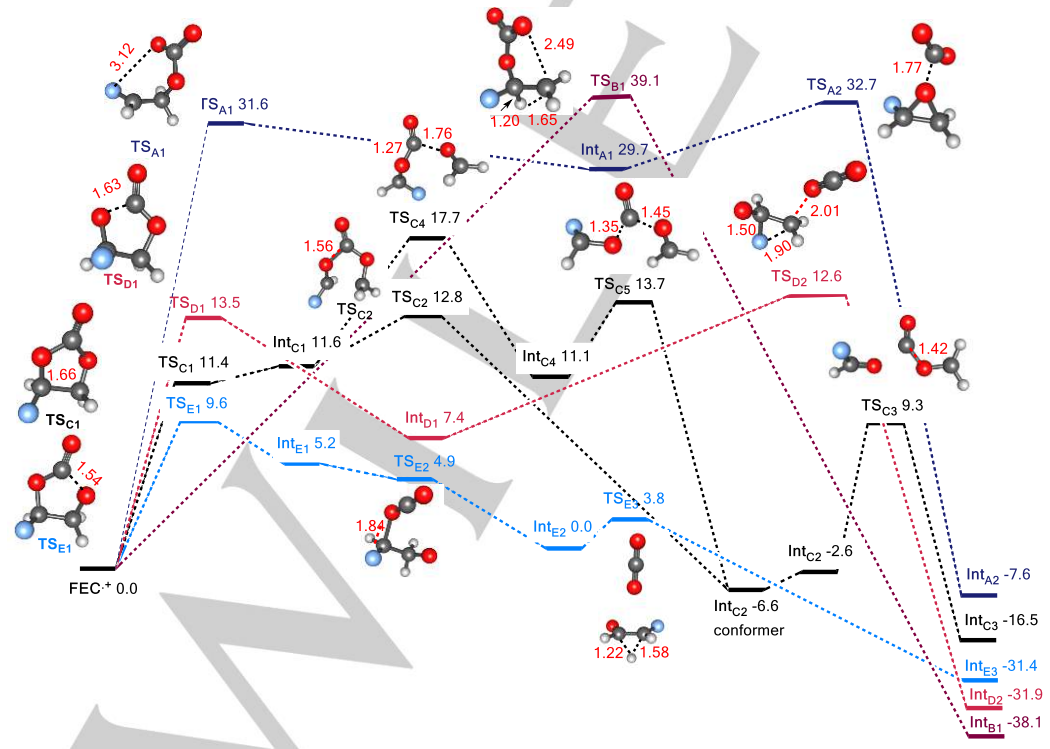

Figure 3. Energy profile for the decomposition of **FEC$^{\bullet+}$** with optimized geometry of transition states at B3LYP/6-311++G (d, p) level. Computed free energy profile (Grel, 298K) kcal mol^{-1}. Bond lengths are in angstrom.

Firstly, we prepare the FEC-based electrolytes with different volume ratio and test their conductivity at room temperature. Figure 4 presents the relationship between the ion conductivity of FEC-based electrolytes 1 M $LiPF_6$/FEC+EMC and the mixing volume ratio of FEC at room temperature. As shown in Figure 4, the conductivity of the FEC-based electrolytes increases as the volume ratio of FEC increases. When the volume ratio of FEC and EMC is 3 to 7, the ionic conductivity of the electrolyte reaches to the maximum value of ~8.88 mS cm^{-1}. Then the conductivity of the FEC-based electrolytes decreases as the volume of FEC increases. According to the literature [30], the conductivity results from the product of the amount of charges multiplied by their mobility. When the kind of solute and its concentration is fixed, charges and their mobility are affected mainly by dielectric constant of solvent and viscosity of solution, respectively. As displayed in Table S1, FEC has high dielectric constant and viscosity while EMC has low dielectric constant (ε=2.958) and low viscosity (0.65 cP at 25ºC). In 1 M $LiPF_6$/FEC+EMC mixed electrolytes system, the dielectric constant linearly increases with an increase in a mixing volume ratio of FEC. However, due to the high viscosity of FEC, the viscosity of the FEC-based electrolytes increases with an increase in the mixing volume ratio of FEC. Therefore, the maximum conductivity of the electrolyte is resulted from the total effects of change in dielectric constant and viscosity. In this paper, we select the high conductive composition, 1 M $LiPF_6$/FEC+EMC (3:7, v/v) as the FEC-based electrolyte in following experiments.

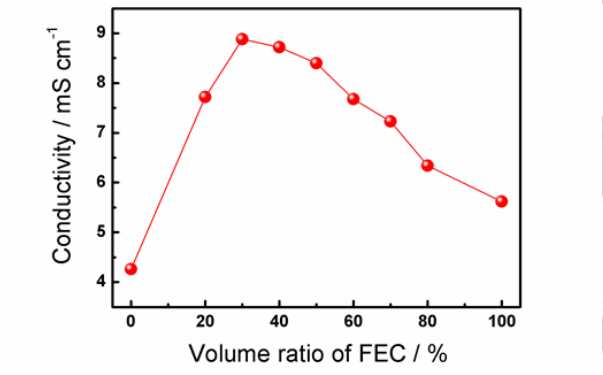

Figure 4. Relationships between volume ratio of FEC in 1 mol L^{-1} $LiPF_6$/FEC+EMC electrolyte and ionic conductivity (25ºC).

To investigate the oxidative stability of the FEC-based electrolytes, Figure 5 gives the cyclic voltammetry (CV) of the FEC-based electrolytes 1 M $LiPF_6$/FEC+EMC (3:7, v/v) at a scan rate of 5 mV s^{-1}, together with the baseline electrolyte 1 M $LiPF_6$/EC+EMC (3:7, v/v) for comparison. As displayed in Figure 5, the baseline electrolyte suffers from the oxidative decomposition above 4.3 V vs. Li^+/Li. However, the oxidation current of the FEC-based electrolytes starts to be oxidized around 5.0 V, exhibiting a greatly high oxidative stability. Therefore, the FEC-based electrolytes demonstrate rather higher oxidative stability compared to that of the EC-based electrolyte, which matches exactly with the DFT calculation results (Table S1). As a conclusion, the enhanced oxidative stability of FEC-based electrolytes is expected to secure superior electrochemical performance for 5 V high voltage cathodes.

:

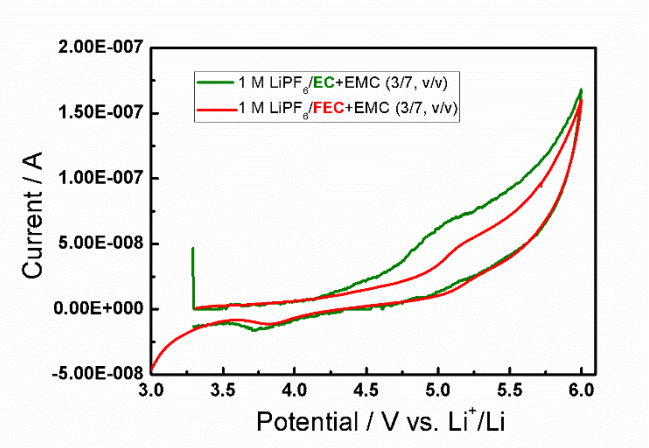

Figure 5. Cyclic voltammagrames of electrolyte solutions 1 mol L^{-1} $LiPF_6$/EC+EMC (3:7, v/v) and 1 mol L^{-1} $LiPF_6$/FEC+EMC (3:7, v/v) using Pt microelectrode, scan rate5 mV s^{-1}.

Figure 6 shows a comparison of the electrochemical behaviors of $LiNi_{0.5}Mn_{1.5}O_4$/Li coin-cells cycled between 3.0 and 5.0 V at 25ºC with two electrolyte solutions (EC- and FEC-based). Figure 6a and 6b show the galvanostatic discharge-charge curves for 1st, 2nd, 5th, 6th, 10th, 20th, 50th and 106th cycles of the $LiNi_{0.5}Mn_{1.5}O_4$/Li cells in two electrolyte solutions. All the electrodes were cycled at 20 mA g^{-1} in the first 5 cycles, and 40 mA g^{-1} for the later cycles. As seen in the curve profile, the $LiNi_{0.5}Mn_{1.5}O_4$/Li cells in the first 5 cycles with the two electrolyte solutions display similar charge-discharge profiles, while the cell has a ~50 mV higher charge voltage in the FEC-based electrolyte than in the EC-based electrolyte, which should be ascribed to the high viscosity of FEC solvent. As the cycle number is elevated from 6th to 106th, the charge voltages of the $LiNi_{0.5}Mn_{1.5}O_4$ cell in the EC-based electrolyte slightly increase, which is associated with the baseline electrolyte decomposition at the high operating voltage to increase interfacial resistance. In contrast, under the same condition with the FEC-based electrolyte, the cell exhibits a highly reversible charge-discharge behavior with a discharge capacity of about 130.4 mAh g^{-1} after 106 cycles, showing a superior cycling performance of the high-voltage battery. Furthermore, Figure 6c shows the capacity retention and coulombic efficiency upon cycling. It can be clearly seen that the cells cycled with the FEC-based electrolyte solution exhibit a capacity retention of almost 100% after 106 cycles, whereas the cells cycled with the EC-based solution show a decrease in the reversible capacity at the end of 106 cycles (capacity retention of 94.3% after 106 cycle). Additionally, Figure 6c also compares the coulombic efficiency of $LiNi_{0.5}Mn_{1.5}O_4$/Li cells with two electrolyte solutions. The FEC-based electrolyte exhibits an obviously

increased initial coulombic efficiency of 94.3% compared to the EC-based electrolyte (88.9%). It is also note that the cell cycled in the FEC-based electrolyte shows a significant improvement in coulombic efficiency of 99.5% during cycling, while the cell cycled with the EC-based solution shows a low coulombic efficiency of 98.5% during cycling. It is assumed that the low coulombic efficiency in EC-based electrolyte solution results from the formation of a solid electrolyte interphase and the electrolyte decomposition at high voltage. These data obviously demonstrate that the FEC-based electrolyte solution exhibits superior electrochemical performance of 5 V high-voltage spinel $LiNi_{0.5}Mn_{1.5}O_4$ electrodes. The improving cyclability of the $LiNi_{0.5}Mn_{1.5}O_4$ electrode can be accounted for by the high oxidative stability of the FEC-based electrolyte solution, which is in accordance with the DFT calculation (Table S1) and CV (Figure 5) results.

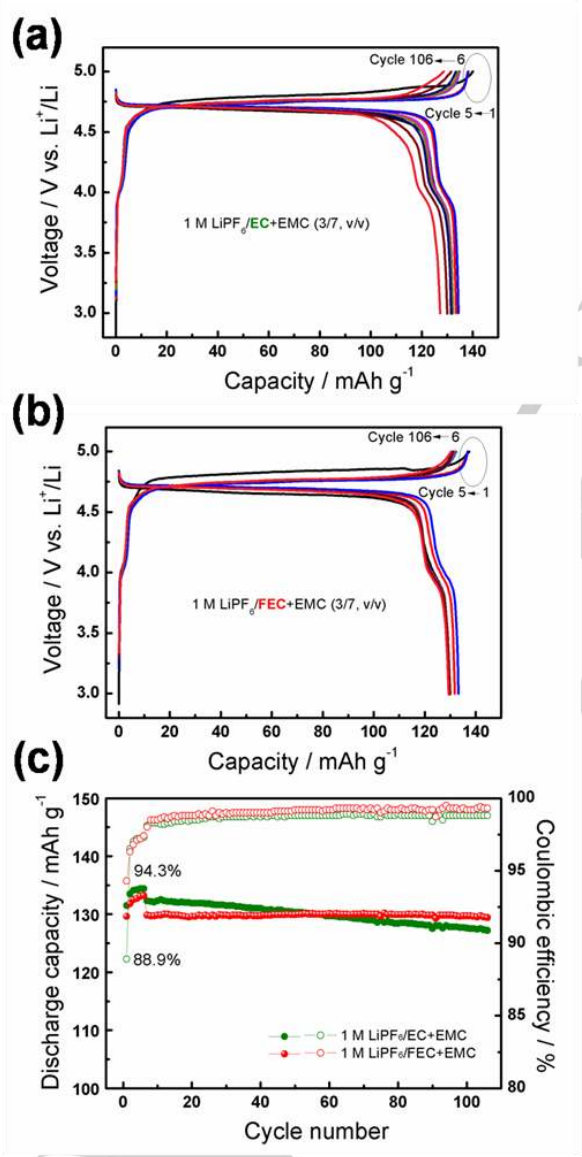

Figure 6. The galvanostatic discharge-charge curves for 1st, 2nd, 5th, 6th, 10th, 20th, 50th and 106th cycles of the $LiNi_{0.5}Mn_{1.5}O_4$/Li cells in EC-based (a) and FEC-based (b) electrolyte solutions, (c) Curves of discharge capacity and coulombic efficiency vs. cycle number obtained upon cycling between 3.0 and 5.0 V for $LiNi_{0.5}Mn_{1.5}O_4$ electrode in these two electrolytes. All the electrodes were cycled at 20 mA g^{-1} in the first 5 cycles and 40 mA g^{-1} for the later cycles.

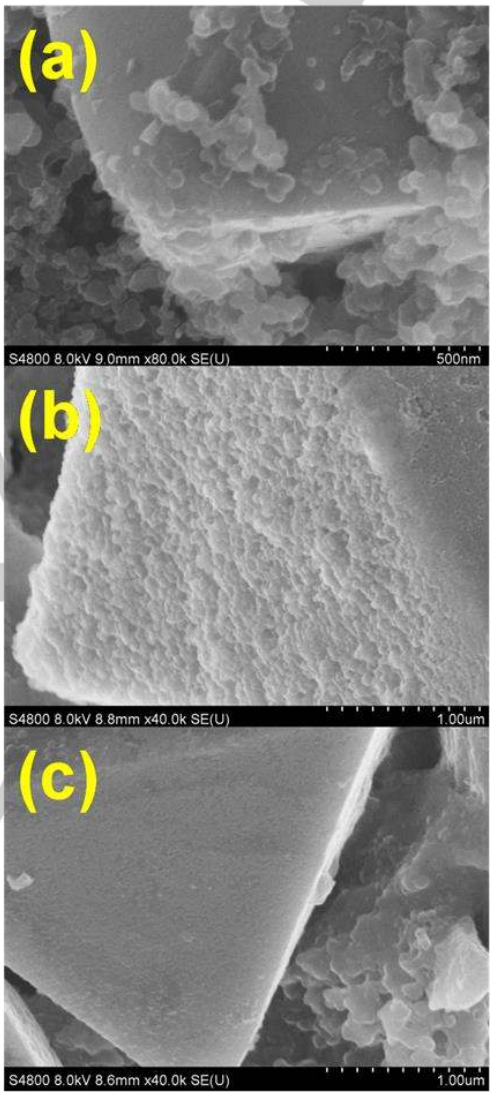

Figure 7. SEM images of (a) pristine $LiNi_{0.5}Mn_{1.5}O_4$ positive electrode and the electrode after 106 cycles with (b) EC-based electrolyte 1 mol L^{-1} $LiPF_6$/EC+EMC (3:7, v/v) and (c) FEC-based electrolyte 1 mol L^{-1} $LiPF_6$/ FEC+EMC (3:7, v/v).

To clarify the interfacial properties of $LiNi_{0.5}Mn_{1.5}O_4$ positive electrode using these two electrolytes, we carried out different testing methods including Scanning electron microscopy (SEM), electrochemical impedance spectroscopy (EIS), and X-ray photoelectron spectroscopy (XPS). Figure 7 compares SEM images of pristine and 106 times cycled $LiNi_{0.5}Mn_{1.5}O_4$ electrodes with two electrolyte solutions (EC-and FEC-based). The SEM image of the pristine electrode (Figure 7a) shows a mixture of

$LiNi_{0.5}Mn_{1.5}O_4$ spinel particle with a very clean surface and their surface containing some carbon black particles and poly (vinylidene fluoride) (PVDF) binder. It can be obviously seen from Figure 7b and 7c that distinct difference was observed of the $LiNi_{0.5}Mn_{1.5}O_4$ electrode cycled in two electrolyte solutions. As shown in Figure 7b, the $LiNi_{0.5}Mn_{1.5}O_4$ electrode cycled with the EC-based electrolyte solution displayed a bumpy surface, and more degradation species were precipitated on the surface of the electrode surface, which may be caused by the baseline electrolyte decomposition products. Based on previous reports [1], it is reasonable that this thick deposit on the electrode would be the **PEC***-like polymeric species, as a result of electrolyte oxidation. On contrast, Figure 7c shows the image of the electrode cycled in the FEC-based electrolyte solution. Compared to Figure 7a, the $LiNi_{0.5}Mn_{1.5}O_4$ particles remain almost clean surfaces without noticeable amount of deposits. These data can be explained by a lesser amount of oxidative decomposition of the FEC-based electrolyte.

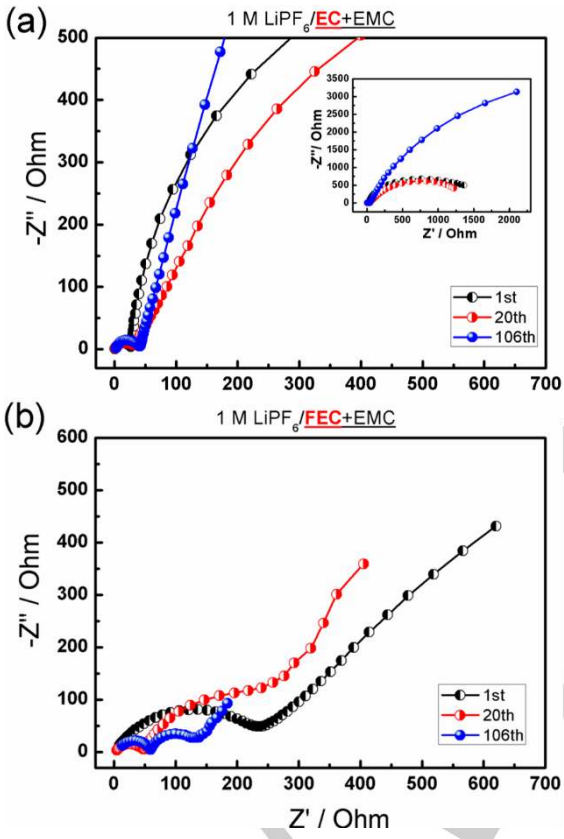

Figure 8. Electrochemical impedance spectra (EIS) curves of the $LiNi_{0.5}Mn_{1.5}O_4$/Li half cells after 1, 20 and 106 cycles with (a) the EC-based electrolyte 1 mol L^{-1} $LiPF_6$/EC+DMC (3:7, v/v) and (b) the FEC-based electrolyte 1 mol L^{-1} $LiPF_6$/ FEC+EMC (3:7, v/v).

To further check the $LiNi_{0.5}Mn_{1.5}O_4$ electrode/electrolyte interface resistance, the EIS spectra were adopted to track the impedance changes after cycling. Figure 8 shows the EIS curves of the $LiNi_{0.5}Mn_{1.5}O_4$/Li coin cells with two electrolyte solutions measured at the 1st, 20th and 106th cycles. The EIS spectra were measured after discharged to 3.0 V. As shown in Figure 8, we can find that all the EIS spectra at high frequencies have two well-defined semicircles, and these two semicircles display the diffusion impedance of Li^+ in the solid electrolyte interphase (SEI) film on cathode surface (R_{SEI}), and interfacial charge transfer resistance (R_{ct}), respectively. After cycling, the cell in the FEC-based electrolyte have lower impedance R_{ct} than that in the EC-based electrolyte, which is possibly due to the better properties of the FEC-derived SEI film on the surface of high-voltage electrodes. Moreover, with the EC-based electrolyte solution, the cell shows a fast impedance growth after 106 cycles, reflecting a rapid increase of the charge transfer resistance (R_{ct}) with increasing cycles (Figure 8a). In contrast, the impedance of the cell with FEC-based electrolyte solutions has obviously decreased after 106 cycles, as shown in Figure 8b. This result can be explained by continuous detrimental reactions of the EC-based electrolyte and formation of the thick surface film on pristine $LiNi_{0.5}Mn_{1.5}O_4$ electrode during cycling at high voltage, which may consequently increase the impedance and lead to inferior cycling ability. The decomposition of the FEC-based electrolyte in high-voltage electrode surface is less, which is totally different from the detrimental decomposition of the EC-based electrolyte.

The effects of FEC on the surface chemistry of the $LiNi_{0.5}Mn_{1.5}O_4$ cathode were carried out by a comparison of the XPS measurements obtained from electrodes cycled in EC- and FEC-based solutions after 106 cycles. XPS is a useful tool to analysis the SEI components on the surface of electrodes [31-33]. Before the XPS measurement, the cycled electrodes were thoroughly washed with pure DMC and dried under vacuum. The C 1s, O 1s, F 1s, Mn 2p and P 2p XPS spectra were record and fitted, as displayed in Figure 9. Quantitative data from XPS spectra of the electrode after 106 cycles with two electrolytes are also given in Table S2. As presented in Table S2, in this two electrolyte solutions, higher amounts of C was observed (in comparison to F, Mn, Ni, P, and Li) in the SEI formed, indicating that the decomposition of organic carbonate solvent is primary process responsible for the SEI film formation on the cathodes. From the C 1s spectra of the cycled cathodes in EC-based electrolytes in the Figure 9a, we can see that the peak at 284.8 eV is due to conductive carbon (Super P carbon black) and other two peaks at 290.5 eV (C-F) and 285.5 eV (C-H) are observed, which belong to PVDF. The peak at 290.5 eV are also assigned to a three –oxygen environment (CO_3-like) of carbon atoms in inorganic carbonates MCO_3 or organic carbonates $ROCO_2R$ or –$(OCO_2R)_n$- (polycarbonates). Also, we observe three peaks at 289.1, 287.9, and 286.2 eV corresponding to O=C-O, C=O and C-O environments of carbon, showing that an amount of carbonaceous species is deposited at the surface of the electrode. The intensity of the C-O peak is greater for electrodes cycled with EC-based electrolytes than electrodes cycled with FEC-based electrolytes. The reason is that PEC* was generated by the decomposition of the base electrolyte up to 5.0 V vs. Li^+/Li, which is in good agreement with the reported results [1]. In addition, we find that these peaks in FEC-based electrolytes slightly shifts to higher binding energy compared to the baseline electrolyte solution, which may be attribute to FEC with the high

electronegativity of the F atom. Meanwhile, analysis of O 1s XPS spectra of these electrodes shows that the relative content of C-O oxygen atoms at 533.5 eV is markedly higher in the case of the FEC-based electrolyte solution, in well agreement with the above results. A comparison between the F 1s spectra of $LiNi_{0.5}Mn_{1.5}O_4$ electrodes cycled in the FEC-based and EC-based solutions shows, in the case of the former, that a new peak at 286 eV is observed (Figure 9c), which relates to C-F containing organic products of FEC transformation [7, 34, 35].

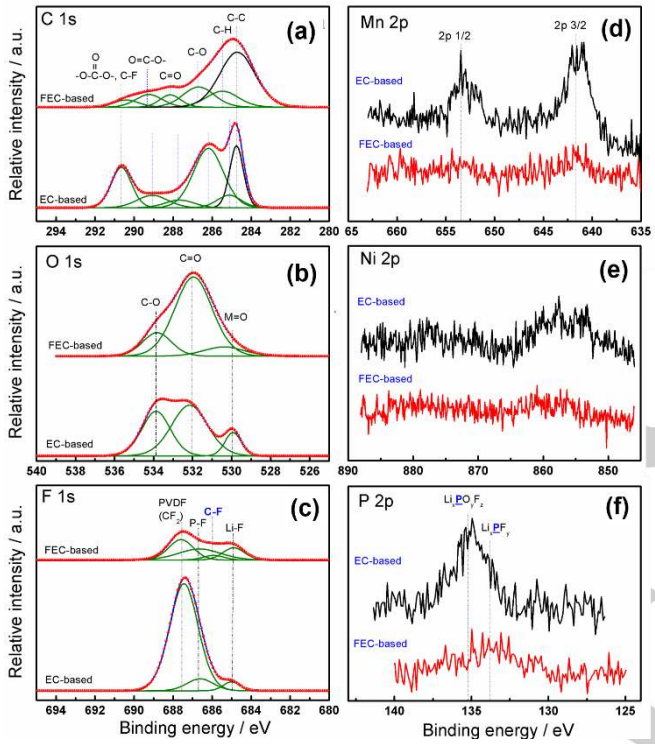

Figure 9. The C 1s, O 1s, F 1s, Mn 2p, Ni 2p and P 2p XPS spectra of the $LiNi_{0.5}Mn_{1.5}O_4$ electrodes with EC- and FEC-based electrolyte solutions collected after 106 cycles.

Figure 9d-f show Mn 2p, Ni 2p and P 2p XPS spectra of the $LiNi_{0.5}Mn_{1.5}O_4$ electrodes with two electrolyte solutions collected after 106 cycles. Because of spin-orbit coupling, each metal 2p spectrum is split in two parts (2p 1/2 and 2p 3/2). As shown in Figure 8d, the Mn 2p spectrum of the $LiNi_{0.5}Mn_{1.5}O_4$ electrode in the EC-based electrolyte displays two peaks at 642.3 eV (2p 3/2) and 654 eV (2p 1/2) in good agreement with the XPS results discussed earlier [24, 36, 37], which may be attributed to the metal Mn ions dissolved from the $LiNi_{0.5}Mn_{1.5}O_4$ electrode in $LiPF_6$-based electrolytes. By contrast, with the FEC-based electrolyte solution, the intensity of the Mn 2p component has almost disappeared after 106 cycles, showing that cycling the $LiNi_{0.5}Mn_{1.5}O_4$ electrode in the FEC-based electrolytes will be beneficial to alleviate the Mn dissolution problem. Similarly, the lower signal of the Ni atoms in the Ni 2p spectrum of the electrodes cycled in the FEC-based electrolytes suggests a lower content of Ni-containing species in the surface film in this case (Figure 8e). It is also worth noting that after 106 cycles, the amount of Mn and Ni species in EC-based electrolytes is much larger than the amount of Mn and Ni species in FEC-based electrolytes analyzed by XPS (Table S2). These results prove that the use of FEC as a cosolvent instead of the commonly used cosolvent EC is efficient to reduce metal dissolution behavior. At the same time, the P 2p spectra in Figure 8f clearly shows peaks for Li_xPF_y (F-P) (at 134 eV) and $Li_xPF_yO_z$ (F-P-O) (at 135.6 eV) in the SEI on the cathodes cycled in the EC-based and FEC-based electrolytes. Li_xPF_y and $Li_xPF_yO_z$ species relate to the decomposition products of $LiPF_6$ salts. However, the intensities of these peaks decreased remarkably for the electrodes cycled in the FEC-based electrolyte solution compared to those cycled in the EC-based electrolyte solution. This is likely because the decomposition of the FEC-based electrolyte upon cycling at high voltage generated less F-P-O and F-P intermediates than that of EC-based electrolytes. Therefore, we conclude that FEC as a cosolvent instead of EC results in a significant decrease of the amount of $LiPF_6$ salts decomposition products in the SEI film at the electrodes surface (less Li and P was also detected in Table S2).

Corroborating SEM, EIS and XPS results, we propose improvement mechanism of the FEC-based electrolyte solution on the $LiNi_{0.5}Mn_{1.5}O_4$ electrode surface. We believe that FEC participates in the surface chemistry of the SEI on the high-voltage $LiNi_{0.5}Mn_{1.5}O_4$ electrode; the resulting SEI effectively blocks further electrolyte solvents and $LiPF_6$ decomposition upon cycling, greatly alleviates the Mn/Ni dissolution from the spinel electrode, and leads to the superior electrochemical performance of the high-voltage $LiNi_{0.5}Mn_{1.5}O_4$ electrode under certain high voltage conditions.

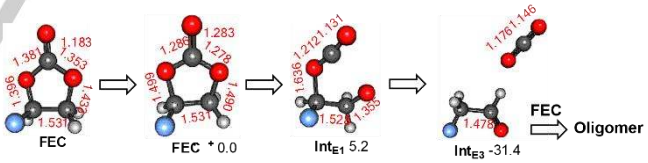

Figure 10. Possible oxidation decomposition mechanism of the FEC solvent.

Conclusions

In summary, similar to the EC-based electrolyte, since FEC in the FEC-based electrolyte easily reaches the surface of positive electrode, FEC is easily to be oxidative in the surface of positive electrode. We have investigated the detailed oxidative decomposition mechanism of FEC using DFT. Radical cation $FEC^{\bullet+}$ is formed from FEC by transferring one electron to electrode and the most likely decomposition products are CO_2 and 2-fluoroacetaldehyde radical cation. Other possible products are CO, formaldehyde and formyl fluoride radical cations. These radical cations are surrounded by much FEC solvent and their radical center may attack the carbonyl carbon of FEC to form

aldehyde and oligomers of alkyl carbonates, which is similar with the oxidative decomposition of EC, as illustrated in Figure 10. Then, we have demonstrated the interfacial film on the high-voltage $LiNi_{0.5}Mn_{1.5}O_4$ electrode using the FEC-based electrolyte solution. The experimental results suggested that robust SEIs formed in FEC-based electrolyte were essential to inhibit unwanted electrolyte solvents and $LiPF_6$ salts decomposition, to alleviate Mn/Ni dissolution, and to preserve the electrochemical properties of high voltage cathodes. This work demonstrates that the FEC-based electrolyte systems have considerable potential replacement of the EC-based electrolyte for the applications in 5 V Li-ion batteries.

Supporting Information Summary

Table S1 and S2. Supporting information also provides the details of computational and experimental methods.

Acknowledgements

We acknowledge financial support by the National Natural Science Foundation of China (21503246 and 21502101), the Natural Science Foundation of Ningbo (2017A610022 and 2017A610070), and the Ningbo Municipal Government (3315 Plan and the IAMET Special Fund, 2014A35001-1).

Keywords: Density functional calculation • Fluoroethylene carbonate • High-voltage • Lithium ion battery • Oxidative decomposition

[1] L. Yang, B. Ravdel, B. L. Lucht, *Electrochem. Solid-State Lett.* **2010**, *13*, A95-A97.
[2] H. Duncan, D. Duguay, Y. Abu-Lebdeh, I. J. Davidson, *J. Electrochem. Soc.* **2011**, *158*, A537-A545.
[3] Z. Zhang, L. Hu, H. Wu, W. Weng, M. Koh, P. C. Redfern, L. A. Curtiss, K. Amine, *Energy Environ. Sci.* **2013**, *6*, 1806-1810.
[4] L. Liao, P. Zuo, Y. Ma, Y. An, G. Yin, Y. Gao, *Electrochim. Acta* **2012**, *74*, 260-266.
[5] B. Liu, B. Li, S. Guan, *Electrochem. Solid-State Lett.* **2012**, 15, A77-A79.
[6] L. Liao, X. Cheng, Y. Ma, P. Zuo, W. Fang, G. Yin, Y. Gao, *Electrochim. Acta* **2013**, *87*, 466-472.
[7] L. Xia, Y. Xia, C. Wang, H. Hu, S. Lee, H. Chen, Z. Liu, *ChemElectroChem* **2015**, *2*, 1707-1712.
[8] T. Kitagawa, K. Azuma, M. Koh, A. Yamauchi, M. Kagawa, H. Sakata, H. Miyawaki, A. Nakazono, H. Arima, M. Yamagata, *Electrochemistry* **2010**, *78*, 345-348.
[9] L. Hu, Z. Zhang, K. Amine, *Electrochem. Commun.* **2013**, *35*, 76-79.
[10] E. Markevich, G. Salitra, K. Fridman, R. Sharabi, G. Gershinsky, A. Garsuch, G. Semrau, M. A. Schmidt, D. Aurbach, *Langmuir* **2014**, *30*, 7414-7424.
[11] M. Xu, S. Dalavi, B. L. Lucht, *in Lithium Batteries: Advanced Technologies and Applications*, ed. B. Scrosati, K. M. Abraham, W. V. Schalkwijk, and J. Hassoun, Wiley, United States, **2013**, *ch. 4*, pp. 71-87.
[12] L. Xing, W. Li, C. Wang, F. Gu, M. Xu, C. Tan, J. Yi, *J. Phys. Chem. B* **2009**, *113*, 16596-16602.
[13] M. G. S. R. Thomas, P. G. Bruce, J. B. Goodenough, *J. Electrochem. Soc.* **1985**, *132*, 1521-1528.
[14] D. Aurbach, K. Gamolsky, B. Markovsky, G. Salitra, Y. Gofer, U. Heider, R. Oesten, M. Schmidt, *J. Electrochem. Soc.* **2000**, *147*, 1322-1331.
[15] W. Li, B. L. Lucht, *J. Electrochem. Soc.* **2006**, *153*, A1617-A1625.
[16] R. S. Assary, L. A. Curtiss, P. C. Redfern, Z. C. Zhang, K. Amine, *J. Phys. Chem. C* **2011**, *115*, 12216−12223.
[17] X. R. Zhang, J. K. Pugh, P. N. Ross, *J. Electrochem. Soc.* **2001**, *148*, E183−E188.
[18] S. Kang, M. H. Park, H. Lee, Y. K. Han, *Electrochem. Commun.* **2012**, *23*, 83−86.
[19] R. L. Wang, L. M. Moshurchak, W. M. Lamanna, M. Bulinski, J. R. Dahn, *J. Electrochem. Soc.* **2008**, *155*, A66–A73.
[20] Y. K. Han, J. Jung, S. Yu, H. Lee, *J. Power Sources* **2009**, *187*, 581−585.
[21] T. Li, L. Xing, W. Li, B. Peng, M. Xu, F. Gu, S. Hu, *J. Phys. Chem. A* **2011**, *115*, 4988−4994.
[22] R. L Wang, C. Buhrmester, J. R. Dahn, *J. Electrochem. Soc.* **2006**, *153*, A445−A449.
[23] M. Ue, A. Murakami, S. Nakamura, *J. Electrochem. Soc.* **2002**, *149*, A1572−A1577.
[24] P. Johansson, *J. Phys. Chem. A* **2007**, *111*, 1378−1379.
[25] L. Xing, O. Borodin, G. D. Smith, W. Li, *J. Phys. Chem. A* **2011**, *115*, 13896− 13905.
[26] O. Borodin, T. R. Jow, *ECS Trans.* **2011**, *33*, 77−84.
[27] L. Xing, C. Wang, W. Li, M. Xu, X. Meng, S. Zhao, J. Phys. Chem. B 2009, 113, 5181-5187.
[28] M. Arakawa, J. Yamaki, *J. Power Sources* 1995, 54, 250-254.
[29] E. G. Leggesse, R. T. Lin, T.-F. Teng, C.-L. Chen, J.-C. Jiang, *J. Phys. Chem. A* 2013, 117, 7959-7969.
[30] K. Xu, *Chem. Rev.* **2004**, *104*, 4303-4418.
[31] J. Xiang, F. Wu, R. Chen, L. Li, H. Yu, *J. Power Sources* **2013**, *233*, 115-120.
[32] N. P. W. Pieczonka, Z. Liu, P. Lu, K. L. Olson, J. Moote, B. R. Powell, J.-H. Kim, *J. Phys. Chem. C* **2013**, *117*, 15947-15957.
[33] K. Ciosek, S. Malmgren, M. Hahlin, H. Rensmo, F. Thébault, P. Johansson, K. Edstrom, *J. Phys. Chem. C* **2013**, *117*, 23476-23486.
[34] A. M. Ferraria, J. D. Lopes da Silva, A. M. Botelho do Rego, *Polymer* **2003**, *44*, 7241-7249.
[35] W. Xu, S. S. S. Vegunta, J. C. Flake, *J. Power Sources* **2011**, *196*, 8583-8589.
[36] Y. Talyosef, B. Markovsky, G. Salitra, D. Aurbach, H. J. Kim, S. Choi, *J. Power Sources* **2005**, *146*, 664-669.
[37] H. Bouayad, Z. Wang, N. Dupré, R. Dedryvère, D. Foix, S. Franger, J.-F. Martin, L. Boutafa, S. Patoux, D. Gonbeau, D. Guyomard, *J. Phys. Chem. C* **2014**, *118*, 4634-4648.

ARTICLE

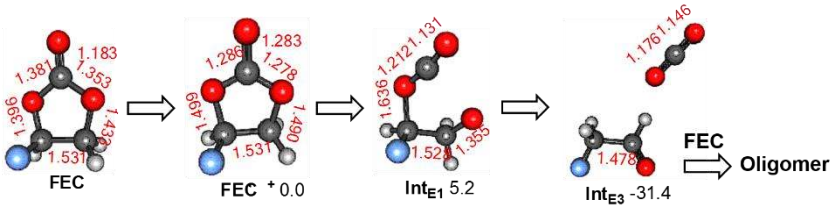

The oxidative decomposition mechanism of FEC used in high-voltage batteries is investigated by using density functional theory (DFT) and experimental study. The most likely decomposition products of FEC are CO_2 and 2-fluoroacetaldehyde radical cation, which can further form aldehyde and oligomers of alkyl carbonates. Our experimental result also reveals that FEC-based electrolyte can form a robust SEI film on the positive electrode surface, which can inhibit unwanted electrolyte solvent and $LiPF_6$ salts decomposition, alleviate Mn/Ni dissolution and therefore, improve the performances of high voltage materials.

L. Xia,[a], [b], [1] B. Tang,[b], [1] L. Yao,[b] K. Wang,[b] A. Cheris,[b] Y. Pan,[b] S. Lee,[a] Y. Xia [a], G. Z. Chen,*[b] Z. Liu[a]*

Page No. – Page No.

Oxidation Decomposition Mechanism of Fluoroethylene Carbonate-Based Electrolytes for High-voltage Lithium Ion Batteries: A DFT Calculation and Experimental Study

WILEY-VCH